Available online at www.sciencedirect.com
SCIENCE DIRECT®
Journal of Sound and Vibration 276 (2004) 671–687
JOURNAL OF SOUND AND VIBRATION
www.elsevier.com/locate/jsvi

Wave propagation in a sensor/actuator diffusion bond model

B.C. Lee[a], M. Palacz[b], M. Krawczuk[b], W. Ostachowicz[b], W.J. Staszewski[a,*]

[a] *Department of Mechanical Engineering, University of Sheffield, Mappin Street, Sheffield S1 3JD, UK*
[b] *Institute of Fluid Flow Machinery, Polish Academy of Sciences, Gdańsk, Poland*

Received 2 September 2002; accepted 4 August 2003

Abstract

Ultrasonic guided waves have been used increasingly in many areas of engineering applications. Often modelling studies are required in order to understand basic principles of different propagation phenomena. Various numerical methods have been used for wave propagation in complex media. This paper reports an application of two recent numerical modelling techniques for wave propagation in a diffusion bond sensor/actuator model consisting of five different layers of material. The spectral elements and local interaction simulation approach are shown to be very attractive modelling tools for guided wave propagation in complex media. Computational efficiency and the ability to model material boundaries are the major advantages of the methods. Numerical simulations are validated using a simple sensor/actuator experiment.

1. Introduction

Waves in solids are important in many engineering applications. This includes elastic and acousto-ultrasonic waves increasingly used for non-destructive damage detection in materials. There are a number of different types of waves used for damage detection. Guided waves, such as Rayleigh and Lamb waves, are particularly attractive for detecting surface defects in plate-like structures. Recent years have shown a number of Lamb wave applications for damage detection in metallic and composite structures [1–4]. These studies often involve piezoceramic sensors embedded in or bonded on structures. Often wave attenuation and/or mode conversion due to damage are used for monitoring. However, a number of other phenomena are observed in propagating waves due to structural discontinuities, boundaries and different properties of complex material layers. It appears that the monitoring strategy and interpretation of damage

*Corresponding author. Fax: +114-22-27890.
E-mail address: w.j.staszewski@sheffield.ac.uk (W.J. Staszewski).

0022-460X/$ - see front matter © 2003 Elsevier Ltd. All rights reserved.
doi:10.1016/j.jsv.2003.08.035

detection results require good understanding of the physical principles behind Lamb wave propagation. Although theoretical principles of Lamb wave propagation are well known in the literature [5,6], analytical approaches are very difficult to use in practice due to complex anisotropy and piezoelectric effects. Therefore a number of numerical techniques are used for wave propagation in complex media.

Wave propagation modelling has attracted many investigations; an excellent overview of numerical techniques is given in Ref. [7]. Previous modelling studies include classical methods of finite difference (FD) [8–10] and finite element (FE) [11–17] analysis. These studies have been extended to boundary element methods (BEM) [18,19] that utilize surface integrals using fundamental solutions in terms of special Green's functions. Other modifications include finite strip elements (FSE) [20,21]. This approach maintains the same matrix principles of the FE analysis but requires much less data storage due to lower level of discretization and polynomial approximations. An excellent summary and application example of matrix techniques for modelling ultrasonic waves is given in Ref. [22]. More recently spectral elements (SE) have been proposed for wave propagation in complex media [23–25]. This global numerical modelling technique performs calculations of the stiffness matrix in the frequency domain. A different approach has been proposed in a mass–spring lattice model (MSLM) [26–28] in which the inertia and stiffness of the analyzed media is modelled using lumped parameters. Recent developments in this area include a new local interaction simulation approach (LISA) [4,29–31]. The method does not use any FD equations but simulates wave propagation heuristically, i.e., directly from physical phenomena and properties.

Guided waves are in general more difficult to model than bulk waves. Relatively less research has been performed on guided wave propagation; examples, mostly using classical matrix-based approaches, include [3,7,8,13]. One-dimensional numerical simulations for wave propagation have been used in practice for various engineering problems as reported for example in Refs. [29,32–34]. However, it appears that very few comparative studies of various modelling techniques of guided wave propagation can be found in the literature. Also, experimental validation of simulation results is not well addressed.

The aim of this paper is to report an application of two recent modelling tools, namely the SE and LISA techniques, for wave propagation in complex media. Both methods are attractive for guided wave propagation modelling. The SE method is a global technique that is easy to implement using the classical FE analysis. The LISA approach is particularly useful to model boundaries and discontinuities between different types of complex media. Both methods are computationally very efficient. The problem of wave propagation, using the SE and LISA approaches, is studied in a sensor/actuator configuration consisting of five different layers of materials with one piezoceramic element generating a thickness mode of vibration. This is also the novelty of the paper; to the best of authors' knowledge the problem has not been analyzed in the literature.

The paper consists of six major parts. A simulated model of actuator/sensor configuration is presented in Section 2. For the sake of completeness, the SE and LISA modelling techniques are briefly described in Sections 3 and 4, respectively. These two sections also include numerical implementations. Wave propagation results are given in Section 5. This includes experimental validation of the simulation results. Finally, the paper is concluded in Section 6.

2. Simulation model of actuator/sensor configuration

Guided waves used for damage detection can be generated using different sources of excitation. Often the actuation is accomplished using piezoceramic actuators and sensors bonded or embedded in the structure. A typical area of application is structural health monitoring (SHM), where Lamb waves are used for damage detection in metallic and composite structures. However, Lamb wave testing is generally complicated by the coexistence of different modes, different experiment configurations and dispersive nature of Lamb waves. As a consequence, response signals used for damage detection are far more complex and often very difficult to interpret. Hence, a detailed numerical analysis of the propagation mechanism is of great interest.

The problem of wave propagation is studied in a sensor/actuator configuration used for damage detection based on acousto-ultrasonic waves. Acousto-ultrasonic techniques utilize stress waves introduced to a structure by a probe at one point and sensed by another probe at a different position. Often bonded piezoelectric ceramic discs are used as probes. One piezoceramic (actuator) element generates a thickness mode of vibration. As a result, a guided wave passes through a couplant and propagates in a monitored specimen, through a couplant, to the second piezoceramic element (sensor), as illustrated in Fig. 1(a). The process of wave propagation associated with this damage monitoring procedure is often studied as problem of wave propagation from point A to B, as shown in Fig. 1(b). However, this configuration does not reflect the actual wave propagation used for damage detection (Fig. 1(a)). Therefore simulated and experimental results exhibit significant differences. Actuator and sensor coupling layers

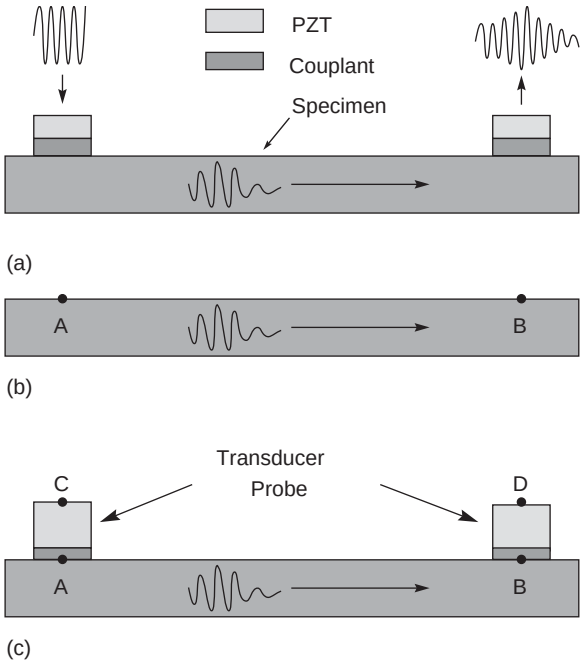

Fig. 1. Lamb wave dispersive propagation studies: (a) general configuration, (b) theoretical configuration and (c) physical wave propagation through couplant configuration.

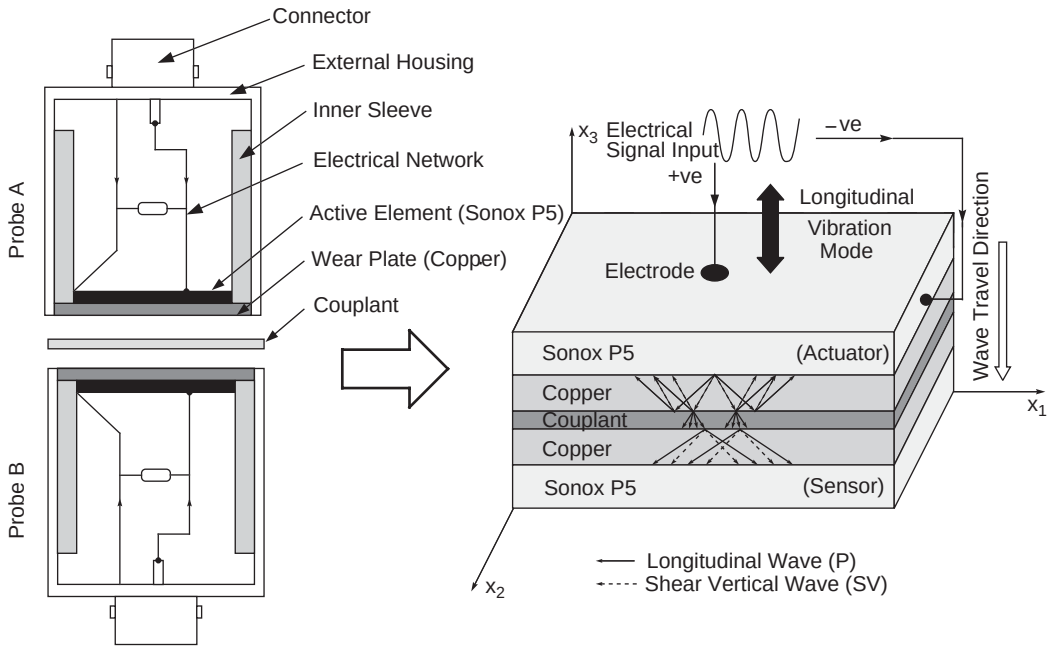

Fig. 2. Procedure of conversion from physical configuration into simulation model.

significantly distort the wave before it leaves and reaches the piezoceramic transducers. Thus it is important to analyze wave dispersion in bonded piezoceramics C and A or B and D, as illustrated in Fig. 1(c).

The problem of wave propagation is studied here in a sensor/actuator diffusion bond model consisting of five different layers of materials. Although this model is similar to two ultrasonic probes coupled together (see Fig. 2), the focus here is on through-thickness wave propagation and not on transducer modelling. The piezoceramic actuator converts the electrical into mechanical energy when the electric field is applied, whereas the piezoceramic sensor converts the mechanical into electrical energy. This is the simplest sensor/actuator configuration available for the experimental study of wave dispersion in various transducer layers. The actual wave propagation in various layers is illustrated in Fig. 2. The top piezoceramic layer generates the thickness mode of vibration resulting in longitudinal (P) and shear vertical (SV) wave propagating in the first copper layer. The energy is further transferred (leaky wave) through the couplant to the second copper and piezoceramic layer. As a result, the wave propagates across various layers of material in the x_3 direction. This wave propagation mechanism is further explained in Ref. [35].

3. Wave propagation modelling using SE

3.1. Spectral elements

The FE analysis is the most widely used approach for wave propagation. The FE matrix approach is based on well-defined elements that are combined together to form analyzed media.

This allows one to study problems of complex geometries, materials and properties. However, the method can lead to expensive computations when large numbers of elements are involved in modelling. Increasing the analyzed frequency range may lead to some uncertainties due to numerical errors. Also, FE analysis is closely related to FD approach in which local variables are used in order to approximate derivatives of functions.

More recently SE analysis has been established as a powerful method used for wave propagation. The spectral element method (SEM), high-accuracy numerical method, combines the accuracy of conventional spectral methods and the geometric flexibility of FE methods. It is the method of Fourier synthesis (or spectral analysis), where the behaviour of the signal is viewed as a superposition of many infinitely long wave trains of different periods (or frequencies). The actual response is synthesized by a judicious combination of these wave trains. Thus the problem of characterizing a signal is transformed into one of determining the set of combination coefficients. These coefficients are called the Fourier transform of the signal. The problem being tackled invariably is simplified when it is expressed in terms of the Fourier transform. The last step in the analysis involves performing an inverse transform (reconstructing the signal).

The SE approach is based on global approximations of functions, i.e., analyzed functions are at first approximated using basis functions and then exactly differentiated. As a consequence, relatively small number of elements can be used for modelling without loosing the accuracy. This is particularly useful for wave propagation modelling.

In this paper one-dimensional wave propagation is considered so a dynamic stiffness relation is established via dynamic shape functions or in other words interpolation functions. These functions describe displacement distribution between spectral element ends. Usually in FE analysis interpolation functions are selected as simple polynomials. In spectral FE methods they are in fact exact displacement distributions.

The spectral analysis approach to wave propagation in a two-dimensional media is the foundation for the spectral element method. To summarize, the analysis begins with the partial differential equations of motion in the scalar and vector potentials Φ and H. These are given for the two-dimensional case as

$$c_p^2 \nabla^2 \Phi(x, y, z, t) = \ddot{\Phi}(x, y, z, t), \tag{1}$$

$$c_s^2 \nabla^2 H(x, y, z, t) = \ddot{H}(x, y, z, t), \tag{2}$$

where the Φ and H potentials correspond to the dilatational and distortional modes [36] with limiting phase speeds of c_p and c_s.

The equation of motion is twice transformed with respect to time and space, for solution in the frequency/wave number domain. The result is an ordinary differential equation with constant coefficients in a single-dependent variable x. The solution is often referred to as the kernel function and the problem is solved by synthesizing the kernels appropriately to satisfy the initial and boundary conditions. Because the subsequent inversion back to the time/space domain is to be performed on a computer, discrete transforms are taken from the outset. The generic solutions have the form:

$$\Phi(x, y, t) = \sum_{n=1}^{N} \sum_{m=0}^{M} \hat{\Phi}_{nm}(x, \eta_m, \omega_n) \begin{Bmatrix} \cos(\eta_m y) \\ \sin(\eta_m y) \end{Bmatrix} e^{i\omega_n t}, \tag{3}$$

$$H(x,y,t)=\sum_{n=1}^{N}\sum_{m=0}^{M}\hat{H}_{nm}(x,\eta_m,\omega_n)\begin{Bmatrix}\cos(\eta_m y)\\ \sin(\eta_m y)\end{Bmatrix}e^{i\omega_n t}, \tag{4}$$

where ω is the angular frequency, η is the horizontal wave number, i is the complex $\sqrt{-1}$. The subscripts n and m are the frequency and wave number indices. For waves propagating in the positive x direction the associated kernels are:

$$\hat{\Phi}_{mn}(x,\eta_m,\omega_n)=A_{mn}e^{-ik_{1mn}x}, \tag{5}$$

$$\hat{H}_{zmn}(x,\eta_m,\omega_n)=B_{mn}e^{-ik_{2mn}x}, \tag{6}$$

where $A_{m,n}$ and $B_{m,n}$ are undetermined coefficients. The wave numbers k_{1mn} and k_{2mn} satisfy the following relations:

$$k_{1mn}=\pm\sqrt{k_{pn}^2-\eta_m^2},\quad k_{pn}\equiv\frac{\omega_n}{c_p}, \tag{7}$$

$$k_{2mn}=\pm\sqrt{k_{sn}^2-\eta_m^2},\quad k_{sn}\equiv\frac{\omega_n}{c_s}. \tag{8}$$

A detailed treatment of these relations is given in Ref. [37]. The coefficients $A_{m,n}$ and $B_{m,n}$ are determined from the applied boundary conditions.

For the analysis performed on the experiment presented in the paper, two SE were used. The first one was a one-node throw-off element and a second one was a two-node layer element. The throw-off element represents a semi-infinite member that acts to conduct energy from the system. The layer element represents a doubly bounded member and is used to model a finite layer.

3.1.1. One-node element

A schematic representation of the one-node (throw-off) element is shown graphically in Fig. 3a. The displacements u and v have the spectral representations:

$$u(x,y,t)=\sum_{n=1}^{N}\sum_{m=0}^{M}\hat{u}_{mn}(x,\eta_m,\omega_n)\begin{Bmatrix}\cos(\eta_m y)\\ \sin(\eta_m y)\end{Bmatrix}e^{i\omega_n t}, \tag{9}$$

$$v(x,y,t)=\sum_{n=1}^{N}\sum_{m=0}^{M}\hat{v}_{mn}(x,\eta_m,\omega_n)\begin{Bmatrix}\cos(\eta_m y)\\ \sin(\eta_m y)\end{Bmatrix}e^{i\omega_n t} \tag{10}$$

with the kernels given as

$$\hat{u}_{mn}(x,\eta_m,\omega_n)=-A_{mn}(ik_{1mn})e^{-ik_{1mn}x}\pm B_{mn}(\eta_m)e^{-ik_{2mn}x}, \tag{11}$$

$$\hat{v}_{mn}(x,\eta_m,\omega_n)=\pm A_{mn}(\eta_m)e^{-ik_{1mn}x}+B_{mn}(ik_{2mn})e^{-ik_{2mn}x}. \tag{12}$$

These equations are analogous to shape functions in conventional FE analysis, but are frequency and wave number dependent. At this stage the formulation is completely general and includes both symmetric and antisymmetric parts. Since the problem of interest is initiated by normal impact, the response is symmetric about $y=0$. Thus, only symmetric terms are included. After including boundary conditions and formulae for spectral nodal forces, the frequency and

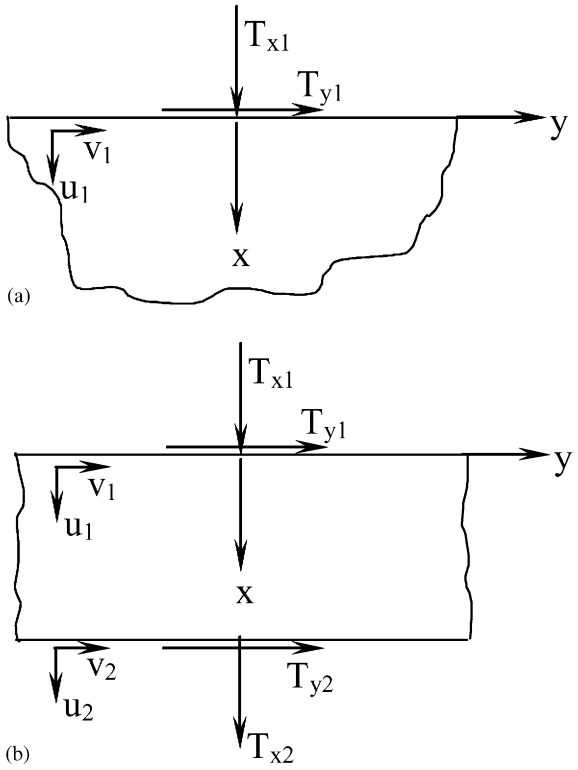

Fig. 3. Sign conventions of: (a) the spectral throw-off element and (b) the layer spectral element.

wave number-dependent dynamic stiffness matrix has the following form:

$$[\hat{\mathbf{k}}_{mn}] = \frac{\mu}{(k_{1mn}k_{2mn} + \eta_m^2)} \begin{bmatrix} \mathrm{i}k_{2mn}k_{sn}^2 & \eta_m(2\eta_m^2 + 2k_{1mn}2_{kmn} - k_{sn}^2) \\ \eta_m(2\eta_m^2 + 2k_{1mn}2_{kmn} - k_{sn}^2) & \mathrm{i}k_{1mn}k_{sn}^2 \end{bmatrix} \tag{13}$$

with μ as the shear coefficient. The (2×2) dynamic stiffness matrix is complex and symmetric.

3.1.2. Two-node layer element

A schematic representation of the spectral layer element is shown graphically in Fig. 3b. The potential kernels are modified as follows to include waves propagating in the negative x direction:

$$\hat{\Phi}_{mn}(x, \eta_m, \omega_n) = A_{mn}\mathrm{e}^{-\mathrm{i}k_{1mn}x} + B_{mn}\mathrm{e}^{-\mathrm{i}k_{1mn}(L-x)}, \tag{14}$$

$$\hat{H}_{zmn}(x, \eta_m, \omega_n) = C_{mn}\mathrm{e}^{-\mathrm{i}k_{2mn}x} + D_{mn}\mathrm{e}^{-\mathrm{i}k_{2mn}(L-x)}, \tag{15}$$

where L is the length of the layer. The displacements u and v have kernels:

$$\hat{u}_{mn}(x, \eta_m, \omega_n) = +[-A_{mn}\mathrm{e}^{-\mathrm{i}k_{1mn}x} + B_{mn}\mathrm{e}^{-\mathrm{i}k_{1mn}(L-x)}](\mathrm{i}k_{1mn}) \pm [C_{mn}\mathrm{e}^{-\mathrm{i}k_{2mn}x} + D_{mn}\mathrm{e}^{-\mathrm{i}k_{2mn}(L-x)}]\eta_m, \tag{16}$$

$$\hat{v}_{mn}(x, \eta_m, \omega_n) = \mp[+A_{mn}\mathrm{e}^{-\mathrm{i}k_{1mn}x} + B_{mn}\mathrm{e}^{-\mathrm{i}k_{1mn}(L-x)}]\eta_m + [+C_{mn}\mathrm{e}^{-\mathrm{i}k_{2mn}x} - D_{mn}\mathrm{e}^{-\mathrm{i}k_{2mn}(L-x)}](\mathrm{i}k_{2mn}). \tag{17}$$

After similar transformation the complex, symmetrical dynamic stiffness matrix can be written in the following form:

$$[\hat{\mathbf{k}}_{mn}] = \begin{bmatrix} k_{11mn} & k_{12mn} & k_{13mn} & k_{14mn} \\ & k_{22mn} & k_{23mn} & k_{24mn} \\ & & k_{33mn} & k_{34mn} \\ sym & & & k_{44mn} \end{bmatrix}, \tag{18}$$

where

$$k_{11mn} = \frac{\mu}{\Delta_{mn}}\left(-\mathrm{i}k_{2mn}k_{sn}^2\right)\left[k_{1mn}k_{2mn}z_{12}z_{21} + \eta_m^4 z_{11}z_{22}\right], \tag{19}$$

$$k_{22mn} = \frac{\mu}{\Delta_{mn}}\left(-\mathrm{i}k_{1mn}k_{sn}^2\right)\left[k_{1mn}k_{2mn}z_{11}z_{22} + \eta_m^4 z_{12}z_{21}\right], \tag{20}$$

$$\begin{aligned} k_{12mn} = {} & \frac{\mu}{\Delta_{mn}}\eta_m k_{1mn}k_{2mn}(-k_{sn}^2 + 4\eta_m^2)[4\mathrm{e}^{-\mathrm{i}k_{1mn}L}\mathrm{e}^{-\mathrm{i}k_{2mn}L} - z_{12}z_{22}] \\ & - \frac{\mu}{\Delta_{mn}}\eta_m[\eta_m^4 - \eta_m^2 k_{2mn}^2 + 2k_{1mn}^2 k_{2mn}^2]z_{11}z_{21}, \end{aligned} \tag{21}$$

$$k_{14mn} = \frac{\mu}{\Delta_{mn}}2\eta_m k_{1mn}k_{2mn}k_{sn}^2[\mathrm{e}^{-\mathrm{i}k_{1mn}L}z_{22} - \mathrm{e}^{-\mathrm{i}k_{2mn}L}z_{12}], \tag{22}$$

$$k_{13mn} = \frac{\mu}{\Delta_{mn}}2\mathrm{i}k_{2mn}k_{sn}^2[k_{1mn}^2 k_{2mn}^2\mathrm{e}^{-\mathrm{i}k_{1mn}L}z_{21} + \eta_m^2\mathrm{e}^{-\mathrm{i}k_{2mn}L}z_{11}], \tag{23}$$

$$k_{24mn} = \frac{\mu}{\Delta_{mn}}2\mathrm{i}k_{1mn}k_{sn}^2[k_{1mn}^2 k_{2mn}^2\mathrm{e}^{-\mathrm{i}k_{2mn}L}z_{11} + \eta_m^2\mathrm{e}^{-\mathrm{i}k_{1mn}L}z_{21}] \tag{24}$$

and

$$\Delta_{mn} = 2\eta_m^2 k_{1mn}k_{2mn}[4\mathrm{e}^{-\mathrm{i}k_{1mn}L}\mathrm{e}^{-\mathrm{i}k_{2mn}L} - z_{12}z_{22}] - [k_{1mn}^2 k_{2mn}^2 + \eta_m^4]z_{11}z_{21}, \tag{25}$$

$$z_{11} = 1 - \mathrm{e}^{-2\mathrm{i}k_{1mn}L}, \quad z_{12} = 1 - \mathrm{e}^{-2\mathrm{i}k_{2mn}L}, z_{21} = 1 + \mathrm{e}^{-2\mathrm{i}k_{1mn}L}, \quad z_{22} = 1 + \mathrm{e}^{-2\mathrm{i}k_{2mn}L}. \tag{26}$$

3.2. Numerical implementation

For wave propagation modelling in a diffusion bond model, described in Section 2, two-node layer elements have been used. The numerical model has been constructed using five elements, where each of the elements has represented material layers of the analyzed sensor/configuration structure, as shown in Fig. 2. One throw-off element has been added at the bottom. The thickness of the top piezoceramic layer was much shorter than the wavelength of the wave excitation frequency, especially for short pulses used in the study. Therefore, it was impossible to introduce the excitation signal to this layer, since destructive interferences in the form of a reflected wave could occur. Although previous studies [6,29] show that these interferences are partially cancelled, an extra source node has been added to the model and a pulse signal has been injected with the advanced time, in order to reduce simulation disturbances. This advanced time depends on the product of wavelength of the excitation signal and the number of pulse cycles used. The dynamic

stiffness matrix has been computed using the fast Fourier transform (FFT) analysis based on 4096 data points. All calculations have been performed in MATLAB® on a PC.

4. Wave propagation modelling using LISA

4.1. Local interaction simulation approach

The LISA is formally similar to the FD approach. However, the associated iteration equations are obtained directly from heuristic considerations. Since local interactions between elements are transferred directly for numerical calculations, therefore wave partial differential equations are bypassed and the algorithm is numerically extremely efficient. Additionally, the LISA already inherits the sharp interface model (SIM), which lowers a number of interface grid points in heterogeneous media. The basic idea of the SIM is to average the interface grid point with the surrounding grid points. The main assumption here is that perfect/smooth contact is maintained between different material layers. The LISA/SIM allows for a more physical and unambiguous treatment of interface discontinuities for different physical layers. The technique has been compared with FDE methods to demonstrate the stability and reliability, particularly in situations where the specimen contains more than one physical property. The results show the LISA/SIM method provides more accurate results with less computer calculations in cases where models come with more than one physical property. The method is also more stable than the classical FDE approach for imperfect material interfaces or heterogeneous materials. This is due to the fact that in the LISA/SIM method the numerical error of the impedance changing across the interface is negligible, if compared with the classical FDE approach which may produce large numerical errors. For the sake of completeness the 2-D LISA approach is described in this section.

The 2-D model consists of elementary cells located in the 2-D Cartesian space (Fig. 4). The cells contain all the physical properties of the analyzed media. Each grid point represents an

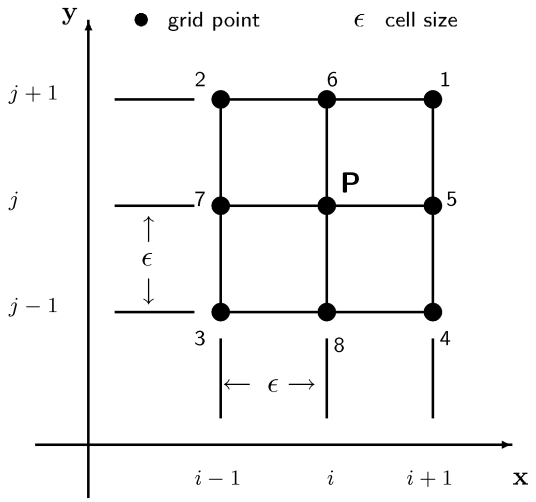

Fig. 4. Space grid for 2-D LISA wave propagation in homogeneous or heterogenous materials.

intersection of four elementary cells. Assuming that the analyzed specimen is orthotropic and symmetrical with respect to the z-axis, the fundamental elastodynamic wave equation for the particle displacement can be given as

$$\partial_l(S_{klmn}\partial_n w_m) = \rho\ddot{w}_k \ (k,l,m,n=1,2), \tag{27}$$

where S is the stiffness tensor, ρ is the density and $\ddot{w}_k$ is the particle displacement.

This equation can be rewritten more explicitly as

$$\partial_k(\sigma_k w_{k,k} + \lambda w_{h,h}) + \partial_h[\mu(w_{k,h} + w_{h,k})] = \rho\ddot{w}_k, \tag{28}$$

where $k = 1,2$ and $h = 3-k$. For simplicity, a square elementary cell of length ε is used. The central intersection point **P** in Fig. 4 is surrounded by eight-node points. This point may contain a maximum of four possible different physical properties.

These are

$$\begin{aligned} \sigma_n^{(k)} &= S_{kkkk}, \quad (k=1,2, n=1,8), \\ \lambda_n &= S_{1122}, \quad (n=1,8), \\ \mu_n &= S_{1212}, \quad (n=1,8), \end{aligned} \tag{29}$$

where k is the number of different types of material and n is the number of nodal points. As a consequence of the SIM approach, the density ρ, shear modulus μ and strain σ can be redefined at the interface as the average values taken from the neighbour cells

$$\begin{aligned} \sigma^{(k)} &= \frac{1}{4}\textstyle\sum_{n=1}^{8}\sigma_n^{(k)}, \quad (k=1,2), \\ \mu &= \frac{1}{4}\textstyle\sum_{n=1}^{8}\mu_n, \quad \rho = \frac{1}{4}\sum_{n=1}^{8}\rho_n. \end{aligned} \tag{30}$$

The above model can be used for both homogeneous and heterogeneous media. In this model, the horizontal (x direction) displacement component u can be obtained from the displacement vector w_1, whereas the vertical (y direction) displacement component v can be derived from the displacement vector w_2. Both displacement values can be given in time as

$$\begin{aligned} u^{t+1} = {} & 2u[1-\chi(\sigma^{(1)}+\mu)] - u^{t-1} + \frac{1}{2}\chi\begin{bmatrix} \sigma_1^{(1)}u_5 + \sigma_2^{(1)}u_7 + \sigma_3^{(1)}u_7 + \sigma_4^{(1)}u_5 \\ +\mu_1 u_6 + \mu_2 u_6 + \mu_3 u_8 + \mu_4 u_8 \end{bmatrix} \\ & + \frac{1}{4}\chi\begin{bmatrix} (\lambda_1+\mu_1)(v_1-v) - (\lambda_2+\mu_2)(v_2-v) \\ +(\lambda_3+\mu_3)(v_3-v) - (\lambda_4-\mu_4)(v_4-v) \\ +(\lambda_1-\mu_1)(v_6-v_5) - (\lambda_2-\mu_2)(v_6-v_7) \\ +(\lambda_3-\mu_3)(v_8-v_7) - (\lambda_4-\mu_4)(v_8-v_5) \end{bmatrix}, \end{aligned} \tag{31a}$$

$$v^{t+1} = 2v[1 - \chi(\sigma^{(2)} + \mu)] - v^{t-1} + \frac{1}{2}\chi \begin{bmatrix} \sigma_1^{(2)} v_6 + \sigma_2^{(2)} v_6 + \sigma_3^{(2)} v_8 + \sigma_4^{(2)} v_8 \\ +\mu_1 v_5 + \mu_2 v_7 + \mu_3 v_7 + \mu_4 v_5 \end{bmatrix}$$
$$+ \frac{1}{4}\chi \begin{bmatrix} (\lambda_1 + \mu_1)(u_1 - u) - (\lambda_2 + \mu_2)(u_2 - u) \\ +(\lambda_3 + \mu_3)(u_3 - u) - (\lambda_4 - \mu_4)(u_4 - u) \\ +(\lambda_1 - \mu_1)(u_5 - u_6) - (\lambda_2 - \mu_2)(u_7 - u_6) \\ +(\lambda_3 - \mu_3)(u_7 - u_8) - (\lambda_4 - \mu_4)(u_5 - u_8) \end{bmatrix}. \tag{31b}$$

The constant χ in the above equation is defined as

$$\chi = \frac{\tau}{\rho\varepsilon^2}, \tag{32}$$

where τ is the time step. In order to ensure that simulation is numerically stable, the model configuration has to satisfy the following condition

$$C = \frac{\tau\sqrt{V_L^2 + V_T^2}}{\varepsilon} \leqslant 1, \tag{33}$$

where V_L is the longitudinal velocity and V_T is the transverse velocity. For attenuative materials the LISA Eq. (31) needs to be rewritten as

$$u^{t+1} = 2uq[1 - \chi(\sigma^{(1)} + \mu)] - qu^{t-1} + \frac{1}{2}\chi q \begin{bmatrix} \sigma_1^{(1)} u_5 + \sigma_2^{(1)} u_7 + \sigma_3^{(1)} u_7 + \sigma_4^{(1)} u_5 \\ +\mu_1 u_6 + \mu_2 u_6 + \mu_3 u_8 + \mu_4 u_8 \end{bmatrix}$$
$$+ \frac{1}{4}\chi q^2 \begin{bmatrix} (\lambda_1 + \mu_1)(v_1 - v) - (\lambda_2 + \mu_2)(v_2 - v) \\ +(\lambda_3 + \mu_3)(v_3 - v) - (\lambda_4 - \mu_4)(v_4 - v) \\ +(\lambda_1 - \mu_1)(v_6 - v_5) - (\lambda_2 - \mu_2)(v_6 - v_7) \\ +(\lambda_3 - \mu_3)(v_8 - v_7) - (\lambda_4 - \mu_4)(v_8 - v_5) \end{bmatrix}, \tag{34a}$$

$$v^{t+1} = 2vq[1 - \chi(\sigma^{(2)} + \mu)] - qv^{t-1} + \frac{1}{2}\chi q \begin{bmatrix} \sigma_1^{(2)} v_6 + \sigma_2^{(2)} v_6 + \sigma_3^{(2)} v_8 + \sigma_4^{(2)} v_8 \\ +\mu_1 v_5 + \mu_2 v_7 + \mu_3 v_7 + \mu_4 v_5 \end{bmatrix}$$
$$+ \frac{1}{4}\chi q^2 \begin{bmatrix} (\lambda_1 + \mu_1)(u_1 - u) - (\lambda_2 + \mu_2)(u_2 - u) \\ +(\lambda_3 + \mu_3)(u_3 - u) - (\lambda_4 - \mu_4)(u_4 - u) \\ +(\lambda_1 - \mu_1)(u_5 - u_6) - (\lambda_2 - \mu_2)(u_7 - u_6) \\ +(\lambda_3 - \mu_3)(u_7 - u_8) - (\lambda_4 - \mu_4)(u_5 - u_8) \end{bmatrix}, \tag{34b}$$

where q is the attenuation parameter.

The current study involves one-dimensional wave propagation. Thus Eq. (34) can be simplified as

$$w_{i,t+1} \approx q(w_{i+1,t} + w_{i-1,t}) - q^2(w_{i,t-1}). \tag{35}$$

This involves a one-dimensional iteration process.

4.2. Numerical implementation

The LISA iteration Eq. (35) for the heterogeneous material and the actuator/sensor diffusion bond model, described in Section 2, has been used in numerical simulations for attenuation and non-attenuation properties. The space grid for the analyzed model included 301 meshing elements. Similarly to SE approach, one extra source layer (first element) has been added to inject an input signal to the sensor/actuator model, as described in Section 3.2. The attenuation parameter q in the coupling layer was assumed to be 0.996. This parameter usually varies as a function of the number of elements in the coupling layer, i.e., the value is proportional to the space grid and inversely proportional to the number of elements. The thickness of the coupling layer was equal to the wavelength divided by eight. This is due to the fact that the theory predicts a continuous wave crossing at octal-wavelength layer and retains reflection until the amplitude gradually decreases to almost zero [38]. The simulation algorithm has been coded using MATLAB® and run on a PC.

5. Wave propagation analysis

5.1. Simulation results

Fig. 5 illustrates the advanced time pulse injection into the model (top part), and the interaction of wave propagation through different material layers. Here the solid line indicates the LISA

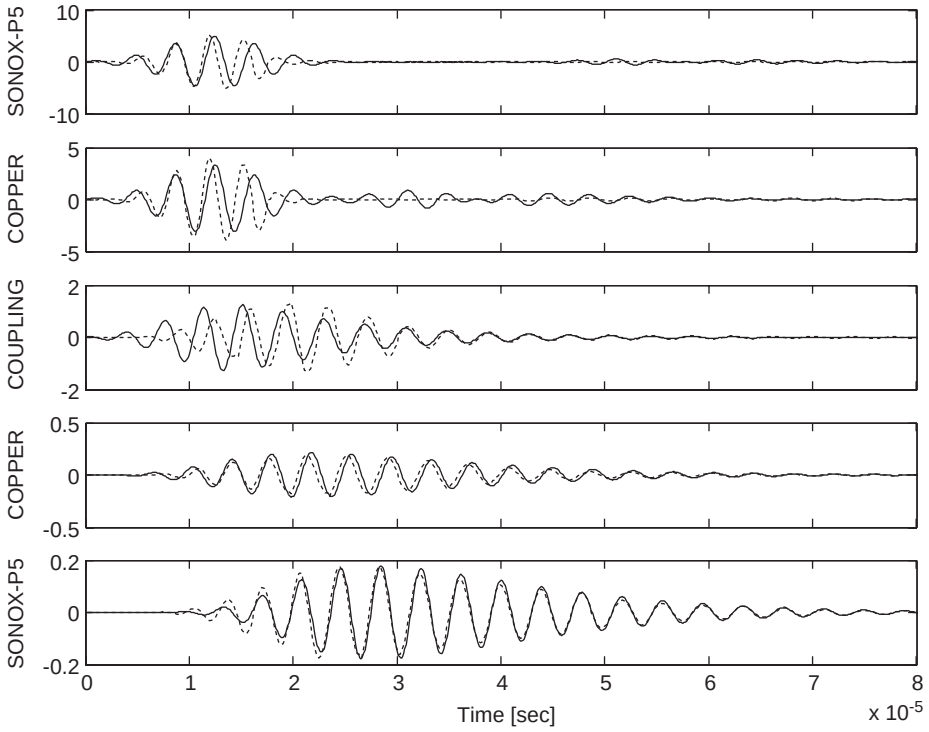

Fig. 5. Lamb wave propagation modelling results: (—) LISA and (- -) SE.

simulation results whereas the dashed line gives the SE simulation results. Two major effects can be observed in the simulated results. These are wave attenuation and wave dispersion. Amplitude reduction can be observed in all material layers. However, the middle-coupling layer absorbs most of the energy before further transmission of the signal to the fourth copper layer. Note that there is some reflection and transmission at the interfaces between copper and coupling layers. As a result, the wave decays exponentially according to the attenuation parameter q. There is no further reflection from both piezoceramic layers. The final signal amplitude, at the bottom piezoceramic layer, is reduced approximately by the factor of 50.

Fig. 5 also illustrates how the five-cycle sine wave propagates into different physical material layers and becomes more dispersive in each layer. Some energy is stored inside the layers. This is consistent with the partial reflection of the pulse from the different material layers and wave energy leakage. Also, the wave velocity changes due to time delay and this results in wave dispersion.

Note that the advanced time pulse injection waves in the first piezoceramic layer are different for both simulation results. This is due to the fact that different methods of injection were applied in both simulation techniques. The SE simulated wave travels faster after crossing the copper/coupling interface and then lags behind the LISA simulated wave after crossing the coupling/copper interface. The piezoceramic/copper and copper/piezoceramic interfaces do not produce such effects. Clearly the other two interfaces involve much more significant differences in the material properties, as shown in Table 1. It appears that the LISA approach copes better with these sharp interfaces. The number of SE in the SE model needs to coincide with the number of discontinuities. Therefore the number of elements in the current simulation was equal to the number of material layers. One extra layer was used to inject the signal, as described in Section 4.2. This resulted in a significant reduction of the matrices involved. The model reduction is the major advantage of the SE method. In contrast, the LISA approach involves 301 elements. However, in two- and three-dimensional simulation the difference between both methods will be less significant.

5.2. Experimental validation

The wave propagation simulation results have been validated using a simple experiment. This involved a similar actuator/sensor configuration to the one described in the simulation model in Section 3. The piezoceramic actuator used in the experimental studies could operate either in S_0 or A_0 Lamb wave mode using excitation frequency equal to 260.5 and 100 kHz, respectively. The frequency of the S_0 mode has been used in this experiment, in order to match the simulated excitation frequency. The excitation signal was generated using the arbitrary function *TTi-TGA*

Table 1
Summary of physical properties used for wave propagation modelling

Layer	Material	Density (kg/m)	Theory velocity (m/s)	Thickness (mm)
1	SONOX-P5	7650	4410	0.5
2	COPPER	8930	4660	0.3
3	COUPLING	870	1740	0.22
4	COPPER	8930	4660	0.3
5	SONOX-P5	7650	4410	0.5

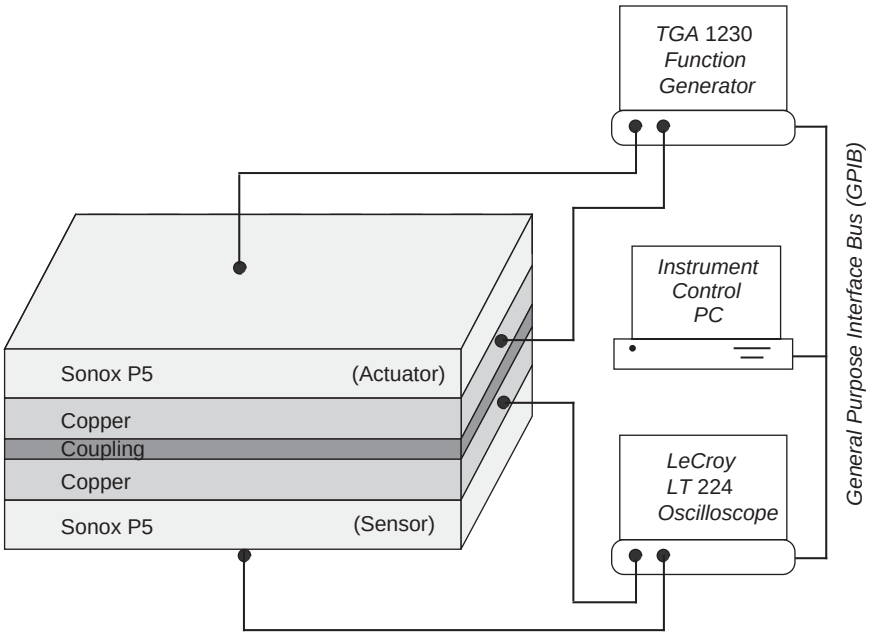

Fig. 6. Experimental set-up for wave propagation studies.

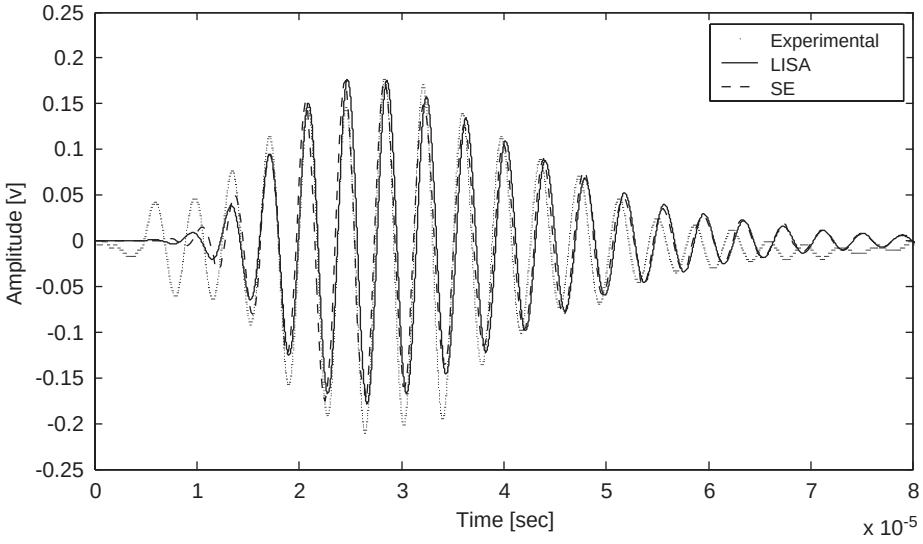

Fig. 7. Comparison between simulated SE (- -), LISA (—) and experimental (. . .) wave propagation results.

1230 signal generator. The wave signal propagated through the layers to the piezoceramic sensor. The *LeCroy Waverunner LT224* oscilloscope was used to display the response from the sensor. Fig. 6 shows the entire experimental set-up.

The comparison between the simulated and experimental results is shown in Fig. 7. Here the solid line gives the LISA simulation results; the dashed line indicates the SE simulation results, whereas the dotted line exhibits the experimental result. Both simulated wave packets are slightly slower and longer than the experimental wave response. This is due to the fact that the five-cycle sine wave used in the experiment has not been modulated with the Hanning window. Nevertheless, a very good agreement between simulated and experimental results can be seen. The mean square error (MSE) defined as y_i is the experiment data point at i location as reference value, and the simulation value at i location is $\widehat{y_i}$.

$$MSE(y) = \frac{100}{N \cdot \sigma_y^2} \sum_{i=1}^{N} (y_i - \widehat{y_i})^2 \tag{36}$$

has been used to compare the experimental and simulated results. Here, y_i and $\widehat{y_i}$ are the experimental and simulated data points for location i, σ_y^2 is the variance of the experimental data which is normalized by N number of data points. The comparison errors are shown in Table 2.

6. Conclusions

Lamb wave propagation in a diffusion bond model has been studied. The model consisted of five different layers of materials with one piezoceramic layer generating the thickness mode vibration. Two numerical simulation techniques, namely spectral elements (SE) and local interaction simulation approach (LISA), have been investigated. Both techniques have been shown to be very attractive modelling tools for guided wave propagation in complex media. Computational efficiency and the ability to model material boundaries are the major advantages of the methods used. It appears that model reduction is the major advantage of the SE analysis. It is known from the literature that the LISA approach is well suited to wave propagation between sharp interfaces. This has been proven again in the paper. Numerical simulations have been validated using a simple sensor/actuator experiment.

Both simulated and experimental studies have shown that the coupling layer distorts the wave packet propagation, due to its low impedance at the interface point and the slow wave speed within the medium. This is vital, especially when piezoceramic sensors and low voltage acousto-ultrasonic inspection are used for damage detection in structures. Thinner coupling layers will not only have less wave attenuation but will also reduce surface coupling between piezoceramics and the analyzed structure. This will influence the reliability of inspection.

Table 2
Summary of statistical comparison between two simulation methods

	Experiment	LISA	SE
Number of grid points	—	301	4096
Mean	−0.008423	0.0006926	−0.00075
Variance	0.004953	0.004079	0.003982
Sum square error		1.3974	0.8689
Mean square error (percentage)	—	26.4623	16.4547

Further studies are required to analyze various wave propagation phenomena and scattering with defects. This should include two-dimensional wave propagation in metallic structures.

Acknowledgements

The work related to the LISA modelling technique, presented in this paper, has been supported by the EPSRC under the research Grant No. GR/N39906/01. The authors would also like to acknowledge the KBN for the financial support of the SE modelling work under the research contract No. 1514/T07/2001/20.

References

[1] N. Guo, P. Cawley, The interaction of Lamb waves with delaminations in composite laminates, *Journal of the Acoustical Society of America* 94 (4) (1993) 2240–2246.
[2] W.J. Staszewski, C. Biemans, C. Boller, G.R. Tomlinson, Crack propagation monitoring in metallic structures, in *Proceedings of the International Conference on Smart Materials Structures, Systems*, Bangalore, India, 1999, pp. 532–541.
[3] S. Beard, F.K. Chang, Active damage detection in filament wound composite tubes using built-in sensors and actuators, *Journal of Intelligent Material Systems and Structures* 8 (1997) 891–897.
[4] V. Agostini, J.C. Baboux, P.P. Delsanto, T. Monnier, D. Olivero, Application of Lamb waves for the characterization of composite plates, in *Proceedings of the Ninth Conference on Non-Destructive Characterization of Materials*, New York, 1999, pp. 455–460.
[5] I.A. Viktorov, *Rayleigh and Lamb Waves—Physical Theory and Applications,*, Plenum, New York, 1967.
[6] J.L. Rose, *Ultrasonic Waves in Solid Media,*, Cambridge University Press, Cambridge, 1999.
[7] L.J. Bond, Numerical techniques and their use to study wave propagation and scattering: a review, in: S.K. Datta, J.D. Achenbach, Y.S. Rajapakse (Eds.), *Elastic Waves and Ultrasonic Nondestructive Evaluation*, North-Holland, Amsterdam, 1990.
[8] J.C. Strickwerda, *Finite Difference Schemes and Partial Differential Equations,*, Wadsworth-Brooks, Belmont, 1989.
[9] Z.S. Alterman, D. Loewenthal, Seismic wave in a quarter and three quarter plane, *Geophysical Journal of the Royal Astronomical Society* 20 (2) (1970) 101–126.
[10] H. Yamawaki, T. Saito, Numerical calculation of surface waves using new nodal equation, *NDT & E International* 8–9 (1992) 379–389.
[11] O.C. Zienkiewicz, The Finite Element Method, 4th Edition, McGraw-Hill, London, 1989.
[12] R.J. Talbot, J.S. Przemieniecki, Finite element analysis of frequency spectra for elastic wave guides, *International Journal of Solids Structures* 11 (1976) 115–138.
[13] M. Koshiba, S. Karakida, M. Suzuki, Finite element analysis of Lamb waves scattering in an elastic plate waveguide, *IEEE Transactions on Sonics and Ultrasonics* 31 (1) (1984) 18–25.
[14] Al-. Nassar, S.K. Datta, A.H. Shah, Scattering of Lamb wave by a normal rectangular strip weldment, *Ultrasonics* 29 (1991) 125–132.
[15] G.S. Verdict, P.H. Gien, C.P. Burger, Finite element study of Lamb wave interactions with holes and through thickness defects in thin metal plates, in: D.O. Thompson, D.E. Chimenti (Eds.), *Review of Progress in Quantitative Nondestractive Evaluation*, Vol. 11, Plenum, New York, 1992, pp. 97–104.
[16] D.N. Alleyne, P. Cawley, Optimization of Lamb wave inspection techniques, *NDT & E International* 25 (C1) (1992) 11–12.
[17] S. Diaz, C. Soutis, Structural integrity monitoring of CFRP laminates using piezoelectric devices, CD proceedings, in *Proceedings of the Ninth European Conference on Composite Materials*, Brighton, UK, 2000.
[18] C.A. Brebbia, J.C.F. Tells, L.C. Wrobel, *Boundary Element Techniques*, Springer, Berlin, 1984.

[19] Y. Cho, J.L. Rose, A boundary element solution for mode conversion study of the edge reflection of Lamb waves, *Journal of the Acoustical Society of America* 99 (4) (1996) 2097–2109.
[20] Y.K. Cheung, *Finite Strip Method in Structural Analysis*, Pergamon Press, Oxford, 1976.
[21] G.R. Liu, J. Tani, K. Watanabe, T. Ohyoshi, Harmonic wave propagation in anisotropic laminated strips, *Journal of Sound and Vibration* 139 (2) (1990) 313–330.
[22] M.J.S. Lowe, Matrix techniques for modeling ultrasonic waves in multilayered media, *IEEE Transactions on Ultrasonics, Ferroelectrics, and Frequency Control* 42 (4) (1995) 525–542.
[23] B. Fornberg, *A Practical Guide to Pseudospectral Methods,*, Cambridge University Press, Cambridge, 1998.
[24] M. Krawczuk, W. Ostachowicz, Spectral finite elements and genetic algorithm for crack detection in cantilever rod, *Key Engineering Materials* 204–205 (2001) 241–250.
[25] W. Ostachowicz, M. Krawczuk, M. Cartmell, M. Gilchrist, Detection of delamination using spectral finite elements, in *Proceedings of the First European Workshop on Structural Health Monitoring*, Paris, France, 2002, pp. 334–351.
[26] P.P. Delsanto, R.B. Mignogna, A spring model for the simulation of the propagation of ultrasonic pulses through imperfect contact interfaces, *Journal of the Acoustical Society of America* 104 (5) (1998) 1–8.
[27] K. Harumi, Computer simulation of ultrasonics in a solid, *NDT & E International* 19 (5) (1986) 315–332.
[28] H. Yim, Y. Sohn, Numerical simulation and visualization of elastic waves using mass–spring lattice model, *IEEE Transactions on Ultrasonics, Ferroelectrics, and Frequency Control* 47 (3) (2000) 549–558.
[29] P.P. Delsanto, T. Whitcombe, H.H. Chaskelis, R.B. Mignogna, Connection machine simulation of ultrasonic wave propagation in materials. I: the one-dimensional case, *Wave Motion* 16 (1992) 65–80.
[30] P.P. Delsanto, R.S. Schechter, H.H. Chaskelis, R.B. Mignogna, R.B. Kline, Connection machine simulation of ultrasonic wave propagation in materials. II: the two-dimensional case, *Wave Motion* 20 (1994) 295–314.
[31] P.P. Delsanto, R.S. Schechter, R.B. Mignogna, Connection machine simulation of ultrasonic wave propagation in materials. III: the three-dimensional case, *Wave Motion* 26 (1997) 329–339.
[32] R.J. Nagem, J.H. Williams, Reflection and transmission of random disturbances at joints in one-dimensional structures, *Mechanics of Structures and Machines* 22 (3) (1994) 327–342.
[33] L.W. Cai, J.H. Williams, One-dimensional modelling of ultrasonic characterization of face sheet-core debonding in composite sandwich panels, *Materials Evaluation* 59 (11) (2001) 1320–1328.
[34] T. Meurer, J. Qu, L.J. Jacobs, One-dimensional pulse propagation in a nonlinear elastic media, *SPIE Proceedings* 4335 (2001) 202–209.
[35] R. Seifried, L.J. Jacobs, J. Qu, Propagation of guided waves in adhesive bonded components, *NDT & E International* 35 (2002) 317–328.
[36] S.A. Rizzi, J.F. Doyle, A spectral element approach to wave motion in a layered solids, *Journal of Vibration and Acoustics* 114 (1992) 569–577.
[37] S.A. Rizzi, J.F. Doyle, Force Identification for Impact of a Layered System, in: R.F. Kulak, L.E. Schwer (Eds.), *Computational aspects of contact, impact and penetration*, Elmepress International, Lausanne, 1991, pp. 222–241.
[38] W.M. Ewing, W.S. Jardetzky, *Elastic Waves in Layered Media,*, McGraw-Hill, New York, 1957.